Effects of a Square Groove at the Stagnation Point of a Circular Cylinder on its Near Wake

Çetin CANPOLAT[1]

[1]*Çukurova Üniversitesi, Mühendislik Mimarlık Fakültesi, Biyomedikal Mühendisliği Bölümü, Adana*

Abstract

In the present study, effects of single longitudinal groove placed at its forward stagnation point on the cylinder wake are investigated. Two different square groove sizes were tested using the particle image velocimetry (PIV) technique and compared with the case of bare cylinder. The cylinders are immersed in a uniform flow field with the Reynolds number, Re=5000. The wakes of these cylinders are evaluated using time-averaged flow data such as vorticity, $\langle\omega\rangle$, streamline, $\langle\Psi\rangle$, components of streamwise, $\langle U/U_o\rangle$ and transverse, $\langle V/U_o\rangle$ dimensionless velocity, Reynolds stresses, $\langle u'v'\rangle$ and turbulent kinetic energy, TKE. In addition, the Strouhal numbers are calculated using frequencies of Karman vortex shedding, which are obtained from single point spectral analysis. It is revealed that the presence of square groove located at forward stagnation point of a circular cylinder has significant effect on the wake formation and turbulence statistics. It is observed that Karman vortex shedding frequency, f_k is also influenced on presence of the groove.

Keywords: Groove, PIV, Turbulence statistics, Vortex shedding

Durma Noktasına Yerleştirilen Bir Çentiğin Silindirin Ölü Akış Bölgesine Etkileri

Özet

Bu çalışmada, bir dairesel silindirin ön durma noktasına yerleştiriliş tekil eksenel çentiğin silindirin ölü akış bölgesine etkileri araştırılmıştır. İki farklı kare kesitli çentik boyutu parçacık görüntülemeli hız ölçme tekniği ile test edilmiş ve çentik olmayan silindir durumu ile karşılaştırılmışlardır. Silindirler Reynolds sayısı, Re=5000 olan serbest akış bölgesine yerleştirilmişlerdir. Bu silindirlerin ölü akış bölgeleri vortisite, $\langle\omega\rangle$, akım çizgileri, $\langle\Psi\rangle$, akım doğrultusundaki, $\langle U/U_o\rangle$ ve akıma dik yöndeki, $\langle V/U_o\rangle$,

---

[1] Yazışmaların yapılacağı yazar: Çetin CANPOLAT, *Mühendislik Mimarlık Fakültesi, Biyomedikal Mühendisliği Bölümü, Adana. ccanpolat@cu.edu.tr*

boyutsuz hız bileşenleri, Reynolds gerilmeleri, $<u'v'>$, ve türbülans kinetik enerji, TKE gibi zaman ortalamalı akış verileri ile incelenmişlerdir. Ek olarak, tekil nokta spektral analizinden elde edilen Karman girdap kopma frekansları kullanılarak Strouhal sayıları hesaplanmıştır. Silindirin ön durma noktasına yerleştirilen kare kesitli çentik ölü akış bölgesinin oluşumuna ve türbülans istatistiklerine önemli etkileri olduğu görülmektedir. Çentiğin Karman girdap kopma frekansının, f_k üzerinde de etkisi olduğu görülmüştür.

Keywords: Çentik, PIV, Türbülans istatistikleri, Girdap kopması

1. INTRODUCTION

The flow past a circular cylinder, which has been studied for many years is one of the fundamental topic of bluff body aerodynamics [1]. The wake of a cylinder is strongly affected by the Reynolds number. Because the cylinder wake, which is formed by the rolling up of two shear layers separating from either side of the cylinder exhibits various features, when the Reynolds number varies. Moreover, the frequency of shear layer separation, which is named as Karman vortex shedding frequency, is also changed by varying Reynolds number. Therefore, circular or nearly circular slender structures are exposed to dynamic loadings due to periodic fluid flow, which deteriorates their integrity and life-time cost in many engineering applications.

The surface properties of a circular cylinder have vital importance on the development of its wake. Leung et al. [2] state that the longitudinal grooves on a cylinder surface change the flow feature, such as drag, lift and vortex shedding frequency. Generally, grooves are utilized for controlling the flow separation and reducing the drag. Corresponding studies in the literature are Kimura and Tsutahara [3], Leung and Ko [4], Leung et al. [5], Lim and Lee [6], Lee et al. [7], Yamagishi and Oki [8], Seo et al. [9]. It is revealed that significant alterations in the boundary layer development and the cylinder wake are observed, when a groove is present. Moreover, drag and the vortex shedding frequency also vary as a function of groove size. In the literature, semi-circular, U-type and V-type grooves are patterned on the circular cylinder surface [2, 4, 6, 7, 9]. The grooves with arc shapes are utilized in the studies of Kimura and

Tsutahara [3] and Yamagishi and Oki [8]. Multiple grooves patterned onto the cylinder surface are generally studied, except Kimura and Tsutahara [3]. They investigate drag reduction around a circular cylinder with single rectangular groove using two dimensional numerical simulation in subcritical Reynolds number regime. Boundary layer separation is also visualized using qualitative dye experiment. It is reported that separation point moves to leading edge of the groove, when the size of the groove increases. Recently, Canpolat [10] studies the effects of size and angular position of a single longitudinally patterned rectangular groove. It is concluded that the parameters tested in this study have substantial importance on the formation of cylinder wake and turbulence statistics. Zhou et al. [1] conduct experimental study to clarify changes in the near wake of circular cylinders with grooved and dimpled surfaces. They concluded that the grooved and dimpled cylinders produce a lower mean drag than that of a smooth cylinder. Moreover, the strength of vortex shedding from the cylinder becomes weaker due to the effect of grooved or dimpled surfaces.

In the open literature, there are various techniques present to suppress flow separation over the bluff bodies. Gad-el-Hak and Bushnell [12] and Lin [13] provide comprehensive reviews about passive flow control methods. The popular passive flow control methods are vortex generators and surface roughness. Vortex generators could be used for the control of flow separation under the flow conditions of supersonic [14], transonic [15], subsonic [16]. The well-known sample for the separation control with surface roughness is golf ball having dimples patterned onto its surface [17]. Achenbach [18] demonstrated the early transition of boundary layer from laminar to turbulent around

a sphere, when it has certain degree of roughness. Moreover, the presence of surface roughness leads to a lower critical Reynolds number than smooth surface. Surface roughness was successfully employed in the studies of Achenbach [19] and Choi et al. [20] for the separation control and drag reduction. However, the surface roughness cannot be used for supersonic separation control like vortex generators.

The current experimental work aims at investigating degree of influence of groove size on the flow characteristics of a circular cylinder. To do this, longitudinally patterned two rectangular grooves with various width-to-depth ratios, such as SQ1= 1 mm x 1 mm and SQ2= 2 mm x 2 mm are tested. The particle image velocimetry (PIV) technique is employed in the present measurements for Re= 5000. Contours of time-averaged/instantaneous vorticity, ω, streamlines, Ψ, streamwise velocity, u/U_o, distributions of turbulence kinetic energy are utilized to present the cylinder wakes. Power spectra of streamwise fluctuating velocity, which provide frequencies of Karman vortex shedding, f_k and small scale waves at specified points on the separated shear layer are also demonstrated.

2. EXPERIMENTAL SET-UP AND PROCEDURE

Particle image velocimetry (PIV) measurements were undertaken in a circulating free-surface water channel with a test section of 8000 mm length, 1000 mm width and 750 mm height. The test section was constructed from transparent 15 mm thick Plexiglas sheet. Water was circulated by a 15 kW centrifugal pump using a speed control unit. Water was pumped through filters and honeycomb arrangement to regulate inertial effects of water and avoid large-scale vortices throughout the test section. Honeycomb arrangement was also utilized for a flow straightener. In order to obtain uniform flow conditions, water enters the test section after smooth channel contraction, which has 1/2 reduction in size. The depth of the water in the test section was adjusted to 600 mm height for the present experiments. Moreover, the

measurements were taken at half depth of water to safely neglect the effects of free-surface of water and bottom wall of the channel. A schematic representation of experimental setup is shown in Figure 1. The turbulence intensity of free-stream flow was about 0.5% for current flow conditions. Reynolds number based on cylinder diameter (D=50 mm) was Re=$5x10^3$ with corresponding uniform flow velocity U_o=100 mm/s for the present investigation. Although the measurement depth is very far away from free surface of water, the Froude number [Fr= $U_o/(ghw)^{1/2}$] is a good proof for presenting the effect of its distortion. The corresponding Froude number is Fr=0.041 which is well below from critical Froude number (Fr<1).

The circular cylinder was made of polyoxymethylene (POM also called as Delrin) type thermoplastic, which has excellent surface smoothness. The groove from tip-to-tip was milled using high precision CNC milling machine. In order to avoid distortion within structure of the material during machining, the length of cylinder was restricted to 300 mm. Both ends of the cylinders were drilled for locating 200 mm long cylinders with same diameter. These additional cylinders were mounted on Plexiglas plates to prevent end effects of cylinder bases (tip vortices) in the cylinder wake. The experiments were conducted at angular position of the groove of θ=0o. The angular position of the groove is defined as relative position of the groove to the forward stagnation point of the cylinder. Sizes of the grooves, which are tested in the current experiments are SQ1= 1 mm x 1 mm and SQ2= 2 mm x 2 mm.
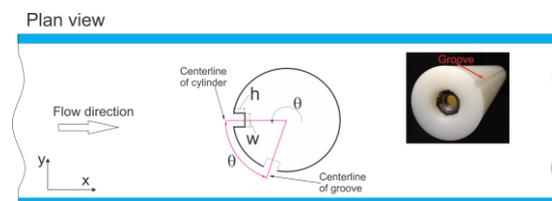
Figure 1. Experimental set-up, parameters and a photo of a cylinder with single groove

Digital PIV system includes a double-pulsed Nd:

YAG Laser source with a wavelength of 532 nm, a 8-bit charged coupled device (CCD) camera, a frame grabber with a maximum frame rate of 30 Hz, a synchronizer and a computer. The time interval between pulses was 1.5 ms and laser sheet had approximately 1.5 mm thick for current experiments. In the case of velocity measurements in the plan view plane, the CCD camera was placed under the water channel. In order to measure flow field perpendicular to camera axis, the laser sheet was oriented parallel to the bottom surface of the water channel. CCD camera was equipped with 60 mm lenses and had resolution of 1600 x 1186 pixels. Silver coated hollow glass spheres with diameter of 12 μm were seeded into water channel. In order to acquire and analyze PIV images, Dantec flow grabber software was utilized. An adaptive correlation technique was employed for computation of instantaneous raw velocity vector fields. The images were interrogated with 32x32 pixels effective windows. The overall field of view was 142.4x106.8 mm^2 and 7227 (99x73) velocity vectors were defined. The magnification factor was determined to be 1:12.03, from the image of a millimeter scale located on the laser sheet in the flow field. An overlap of 50% was utilized in order to satisfy Nyquist criterion for interrogation process. The flow field was analyzed with 1500 images at 15 Hz. Time-averaging were applied to instantaneous images to generate mean flow domain independent from time. Spurious velocity vectors (less than 2%) were removed using the local median-filter technique and replaced by using a bilinear least square fit technique between surrounding vectors. The velocity vector field was also smoothed to avoid dramatic changes in the velocity field using the Gaussian smoothing technique. The vorticity value at each grid point was calculated from the circulation around the eight neighboring points. Uncertainty in velocity measurements is generally caused by the seeding particle size, non-uniform particle distribution, particle overlap, interrogation window size and electronic and optical image noise. In the current study, the number of particle images in an interrogation window was kept between 15 and 20, in order to satisfy the high-image-density criterion. The PIV technique used in this study was similar to the one employed by

Sahin et al. [21], the uncertainty in the velocity field was calculated about 2%. The vorticity magnitude at each grid point was determined from the circulation around the eight neighboring points. In order to check the consistency of experimental results, all experiments, including smooth and grooved cylinder cases, were repeated three times. Contours of time-averaged/instantaneous vorticity, ω, streamlines, Ψ, streamwise velocity, u/Uo, distributions of turbulence kinetic energy, TKE and RMS of streamwise, urms and transverse, vrms velocity fluctuations of each data set were compared and reliability of the data was verified.

3. RESULTS AND DISCUSSIONS

Patterns of time-averaged streamline, <Ψ> of bare cylinder and grooved cylinders indicated as SQ1 and SQ2 are presented in Figure 2 to provide typical flow topology of near wake flow structure of the cylinder. Time-averaged streamlines, Ψ are composed of a pair of focus, F and a saddle point, S further downstream, which are obviously seen in Figure 2. In the present study, a saddle point, S exists at a distance of 1.32D from surface of the smooth cylinder, which agrees well with the literature [22, 23]. In all cases illustrated in Figure 2, symmetry is evident at both side of horizontal axis passing through the cylinder center. In order to present variation of horizontal extent of foci, F and saddle points, S with groove size, a graph is plotted using dimensionless horizontal distance of these points from cylinder center and cylinder diameter. As seen in Figure 2, the horizontal extent of these points belonging SQ2 are the lowest. It is concluded that locations of these points in the circulation region move to the cylinder surface as the groove size increases.

Time-averaged vorticity, ω which is called as the curl of velocity field, components of time-averaged streamwise and transverse velocity are depicted in Figure 3. The corresponding vorticity patterns, <ω> includes positively and negatively rotated layers emanating from forward stagnation point of the cylinder. For the current flow conditions, a wide separated flow region is occurred. The symmetrical distribution along flow

direction is also valid for patterns of time-averaged vorticity. The length of these contours also shrinks in horizontal direction, as the groove size increases. In addition, the magnitudes of maximum vorticity of grooved cylinders are slightly higher than that of bare cylinder. In the second column of Figure 2, streamwise component of dimensionless time-averaged velocity, $<U/U_o>$ are illustrated. Negatively rotated contours are present in the near wake of the cylinder. The location of maximum point of negatively rotated contours move upstream and their magnitudes decrease, when the groove size increases. In the second column of same figure, transverse component of dimensionless time-averaged velocity, $<V/U_o>$ are demonstrated. The maximum magnitudes of $<V/U_o>$ increase with the presence of the groove. However, there is no obvious rise in the maximum magnitude of $<V/U_o>$ as the groove size increases.
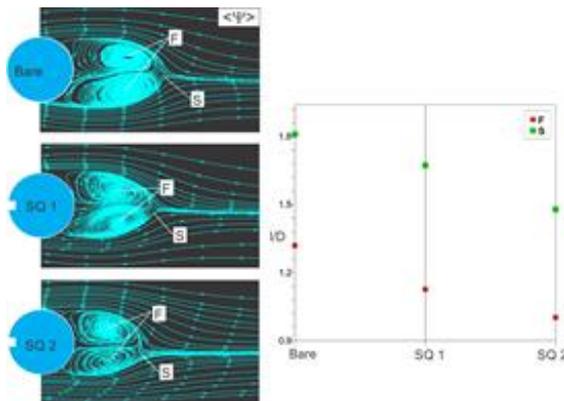
Figure 2. Patterns of time-averaged streamline, $< \Psi >$ for various groove size and a plot showing dimensionless distance between critical points and cylinder center in horizontal direction.

Patterns of Reynold stress correlations, $<u'v'>$ and turbulent kinetic energy, TKE distributions are depicted in Figure 4. The color bar at the top of each column show the magnitude of corresponding statistics. In the first column of Figure 4, well-defined positively and negatively rotated contours are detected. Similar to distributions of vorticity and corresponding streamline, the locations of maxima of Reynold stress correlations move in the upstream direction, when the groove is present. In addition, the maxima of $<u'v'>$ of bare cylinder is lower than that of grooved cylinders. But, there is no significant alteration occurs, when the groove size is varied. In the second column of Figure 4, turbulent kinetic energy, TKE distributions within the near wake of cylinders are illustrated.

Turbulence kinetic energy distributions have single maxima in all cases. Similar to the distributions of $<u'v'>$, the maximum magnitudes of TKE belonging the grooved cylinder have always higher values than bare cylinder.

Moreover, the groove size have no significant effect on maximum values of TKE. The spatial locations of maxima of TKE contours move close to the cylinder surface, as the groove size increases.

Vortex shedding from each side of a circular cylinder causes a well-defined Karman vortex street. Frequency of vorticity pairs is a function of diameter of circular cylinder and the Reynolds number [24]. In the present experiments, power spectra of streamwise fluctuating velocity at single point on separated shear layer indicates one dominant frequency, which is Karman vortex shedding frequency with a magnitude of $f_k=0,38Hz$. This frequency value yields to Strouhal number $St=(f_k \; D)/U_o=0,19$ for current test conditions. Here, D is diameter of the circular cylinder and U_o is the uniform flow velocity. Single peaks are detected at either side of the cylinder, when the groove is present.

The vortex shedding frequency increases slightly and takes $f_k=0,40Hz$ for grooved cylinder. It is concluded that the groove size has no influence on the vortex shedding frequency, when the groove is located at the forward stagnation point of a circular cylinder. The related plots and spatial locations of point used for single point spectral analysis are shown in Figure 5.
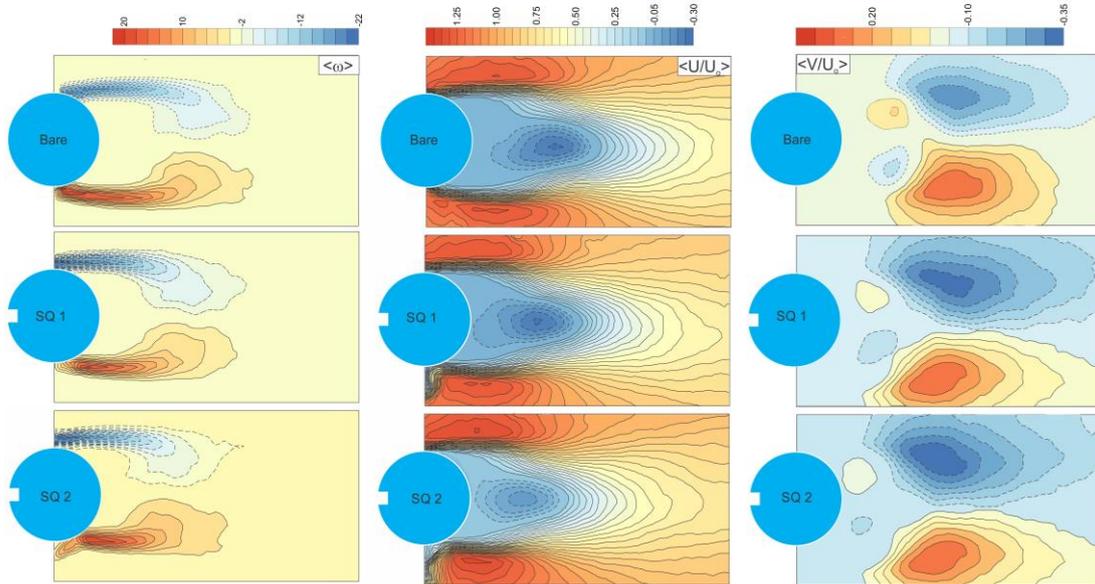
Figure 3. Patterns of time-averaged vorticity,$<\omega>$, streamwise, $<U/U_o>$ and transverse, $<V/U_o>$ components of dimensionless time-averaged velocity for bare and grooved cylinders.
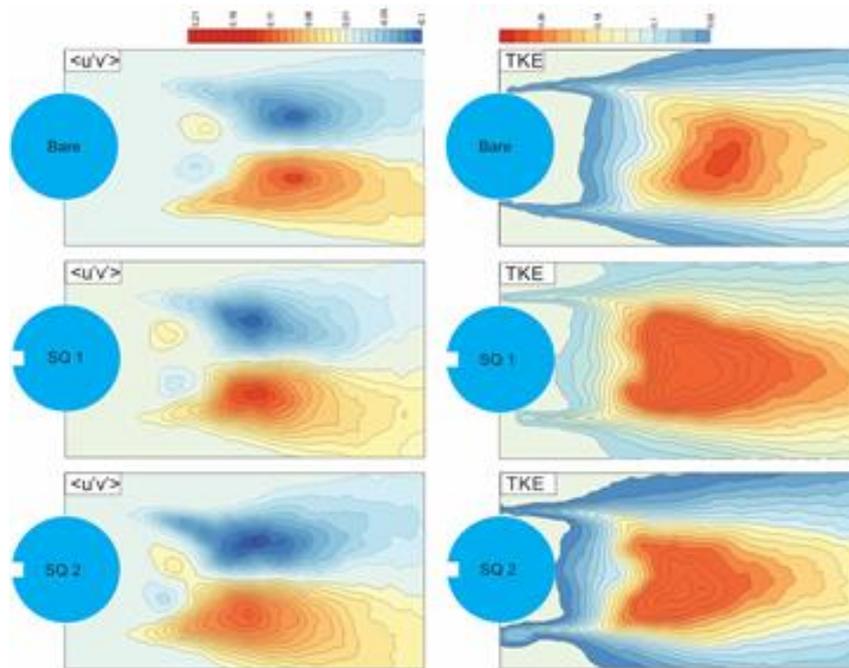
Figure 4. Distributions of Reynolds stresses, $<u'v'>$ and turbulence kinetic energy, TKE for bare and grooved cylinders.
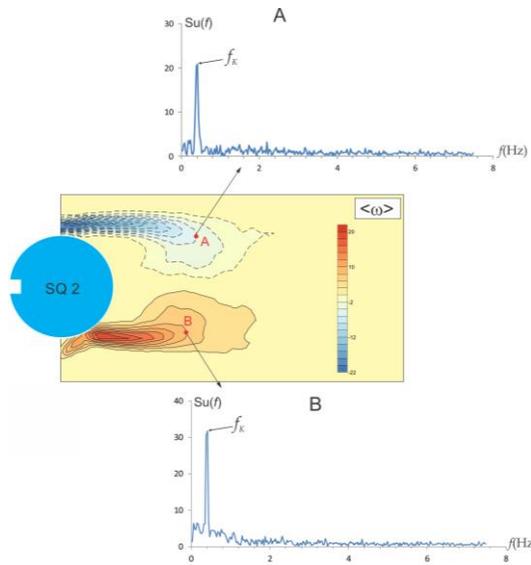
Figure 5. Power spectra of streamwise fluctuating velocity at various locations in the flow field. Karman frequency is indicated with f_k on the graphs

4. CONCLUSIONS

In the present study, flow past a circular cylinder is investigated experimentally as a function of groove size, when the groove is located at the forward stagnation point of the cylinder using the particle image velocimetry (PIV) technique. The influences of flow structure on near wake flow structure and turbulence statistics are revealed with and time-averaged data at Re=5000. Experimental results corresponding bare cylinder (without groove) are well consistent with related literature. In all cases, a symmetry is evident at both side of horizontal axis passing through the cylinder center. Spatial locations of critical points in the circulation region and maxima of turbulence statistics move to the cylinder surface as the groove size increases. However, the groove size has no significant influence magnitudes of maxima of turbulence statistics. The presence of a groove at the forward stagnation point of circular cylinder increases the vortex shedding frequency slightly; but groove size does not create any variation on the same frequency values.

6. REFERENCES

1. Roshko A. 1993. Perspectives on Bluff Body Aerodynamics. Journal of Wind Engineering and Industrial Aerodynamics 49:79-100.
2. Leung Y.C., Wong C.H., Ko N.W.M. 1997. Characteristics of Flows Over an Asymmetrically Grooved Circular Cylinder in the Transitional Regimes. Journal of Wind Engineering and Industrial Aerodynamics 69-71: 169-178.
3. Kimura T., Tsutahara M., 1990. Fluid Dynamic Effects of Grooves on Circular Cylinder Surface. AIAA Journal 29:2062-2068.
4. Leung Y.C., Ko N.W.M. 1991. Near Wall Characteristics of Flow Over Grooved Circular Cylinder. Experiments in Fluids 10:322-332.
5. Leung Y.C., Ko N.W.M., Tang K.M. 1992. Flow Past Circular Cylinder with Different Surface Configurations. Trans. ASME-Journal of Fluids Engineering 114: 170-177.
6. Lim H.C., Lee S.J. 2002. Flow Control of Circular Cylinder with Longitudinal Grooved Surfaces. AIAA Journal 40:2027-2036,
7. Lee S.J., Lim H.C., Han M., Lee S.S. 2005. Flow Control of Circular Cylinder with a V-Grooved Micro-Riblet Film. Fluid Dynamics Research 37:246-266.
8. Yamagashi Y., Oki M. 2007. Numerical Simulation of Flow Around a Circular Cylinder with Curved Sectional Grooves. Journal of Visualization 10:179-186.
9. Seo S-H., Nam C-D., Jan J-Y., Hong C-H. 2013. Drag Reduction of a Bluff Body by Grooves Laid Out by Design of Experiment. Trans. ASME-Journal of Fluids Engineering 135: 111202-1-10.
10. Canpolat C. 2015. Characteristics of Flow Past a Circular Cylinder with a Rectangular Groove.

Flow Measurement and Instrumentation, 45:233-246.

11. Zhou B., Wang X., Guo W., Gho W.M., Tan S.K. 2015. Experimental Study on Flow Past a Circular Cylinder with Rough Surface. Ocean Engineering, 109:7-13.

12. Gad-el-Hak M., Bushnell D.M. 1991. Separation Control. Trans. ASME-J Fluids Eng 113:5-30.

13. Lin J.C. 2002. Review of Research on Low-Profile Vortex Generators to Control Boundary-Layer Separation. Progress in Aerospace Sciences 38:389-420.

14. Souverein L.J., Debieve J.F. 2010. Effect of Air Jet Vortex Generators on a Shock Wave Boundary Layer Interaction Experiments of Fluids 49:1053-1064.

15. Bur R., Coponet D., Carpels Y. 2009. Separation Control by Vortex Generator Devices in a Transonic Channel Flow. Shock Waves 19:521-530.

16. Lin J.C., Robinson S.K., McGhee R.J., Valarezo W.O. 1994. Separation Control on High-Lift Airfoils Via Micro-Vortex Generators. Journal of Aircraft 31:1317–1323.

17. Choi J., Jeon W.P., Choi H. 2008. Control of Flow Over a Bluff Body. Annual Review Fluid Mechanics 40:113-139,

18. Achenbach E. Experiments on the flow Past Spheres at Very High Reynolds Numbers. J. Fluid Mech. 54:565–75,1972.

19. Achenbach E. 1974. The Effect of Surface Roughness and Tunnel Blockage on the Flow Past Spheres. J. Fluid Mech. 65:113–25.

20. Choi J., Jeon W.P., Choi H. 2006. Mechanism of Drag Reduction by Dimples on a Sphere. Physics of Fluids 18:041702.

21. Sahin B., Ozturk N.A., Akilli H. 2007. Horseshoe Vortex System in the Vicinity of The Vertical Cylinder Mounted on a Flat Plate. Flow Measurement and Instrumentation 18:57-68.

22. Parnaudeau P., Carlier J., Heitz D., 2008. Lamballais E. Experimental and Numerical Studies of the Flow Over a Circular Cylinder at Reynolds Number 3900. Physics of Fluids. 20:085101-1-14.

23. Dong S., Karniadakis G.E., Ekmekci A., Rockwell D., 2006. A Combined Direct Numerical Simulation-Particle Image Velocimetry Study of the Turbulent Near Wake. Journal of Fluid Mechanics 569:185-207,

24. Williamson C.H.K., 1996. Vortex Dynamics in the Cylinder Wake. Annual Review Fluid Mechanics 28:477-539.